EFFECTS OF SHEAR LAG ON THERMAL EXPANSION OF 3D CARBON-CARBON COMPOSITES

Julius Jortner
Jortner Research & Engineering, Inc.
Costa Mesa, California

ABSTRACT

The thermal expansion of coupons of 3D carbon-carbon is analyzed in terms of the thermo-elastic properties of the mini-constituents (yarn bundles and matrix pockets) and the stress transfer across their interfaces. The weakness of the interfaces limits the stress transfer by shear. When the shear strength of the interface is exceeded and debonding occurs, stress transfer in the de-bonded region is assumed to be frictional. The frictional shear capability is estimated as a function of the inter-constituent stresses that occur on heating. The analysis, which deals with the stress-transfer using a shear-lag approach, provides estimates of the displacements between mini-constituents. Numerical results are presented to show how elastic and frictional shear lag influences measurements of thermal expansion. The relation of specimen dimensions to the geometry of the composite's unit cell, and details of the measurement technique, are predicted to influence the measured expansions; for some techniques, the measured expansion is predicted to differ significantly from the true expansion of the bulk composite material. Analytical predictions are shown to compare reasonably well to Lander's data on end effects, up to about 4000 F, beyond which the likelihood of creep/relaxation phenomena makes the analysis inapplicable. Directions for improving the analysis are described, and requirements for experimental determination of input properties are identified. Recommendations for accurate thermal expansion testing are provided.

INTRODUCTION

Thermal expansion is usually measured by observing the change in length of a uniformly heated rod or bar of material. For many materials, those having a microstructural dimension that is small enough that the material may be viewed as homogeneous on the scale of the specimen rod or bar, the length change in the test is a direct measure of the thermal expansion of the bulk material. However, for 3D carbon-carbon composites, the cross-sectional dimension of the yarns is in the order of 1 mm, which is not very small compared to the dimensions of typical specimens. Insofar as the composite's thermal expansion depends on stress interactions among the various yarns and the matrix pockets, and insofar as these stresses are influenced by the presence of free surfaces at the boundaries of the specimen, the specimen's change in length is not necessarily a direct measure of the thermal expansion of the bulk composite.

The analysis presented in this paper is intended to model stress transfer between constituents of a 3D composite near free surfaces and its effects on the length changes that would be measured in a thermal expansion test. The inputs to the analysis include the thermo-elastic properties of the mini-constituents, as the yarn bundles and matrix pockets are sometimes called, the strength of the interface between a yarn and the rest of the composite, the dimensions of the composite's unit cell, and the length of the specimen. Outputs include the change in specimen length on heating, as a function of how it is measured, and the stresses generated by heating within the yarn and the surrounding composite. Recommendations for avoiding large errors in estimating thermal expansion of the composite can be derived from the results.

SHEAR LAG ANALYSIS

As shown in Figure 1, the 3D composite is considered to consist of two phases: "yarn", comprising the primary bundles that are oriented axially (normal to the free surface), and "matrix" comprising the other yarn bundles and the matrix pockets. When the composite is heated, differences in the thermal expansions of the two phases give rise to stresses. Generally, on heating of carbon-carbons, the yarn will be in axial tension while the matrix will be in axial compression; perpendicular to the axis, in the transverse direction, the yarn will be in compression (Ref. 1 and 2, for example). At the free surface, in the absence of externally applied tractions, the stresses in yarn and matrix will be zero. Thus, there is a region near the surface in which the stresses vary, which implies the existence of shear at the interface between yarn and matrix. The analysis

Prepared for presentation to the Sixth Rocket Nozzle Technology Meeting of the JANNAF RNTS, Huntsville, 6 December 1984.

Based on research sponsored by the Office of Naval Research under Contract N00014-82-C-0405.

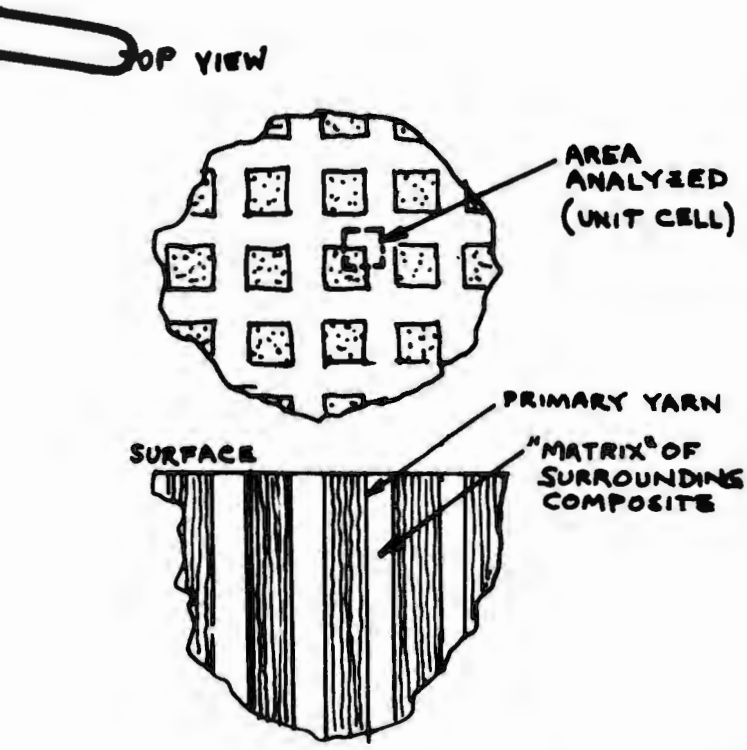

Fig. 1. Idealization of 3D composite.

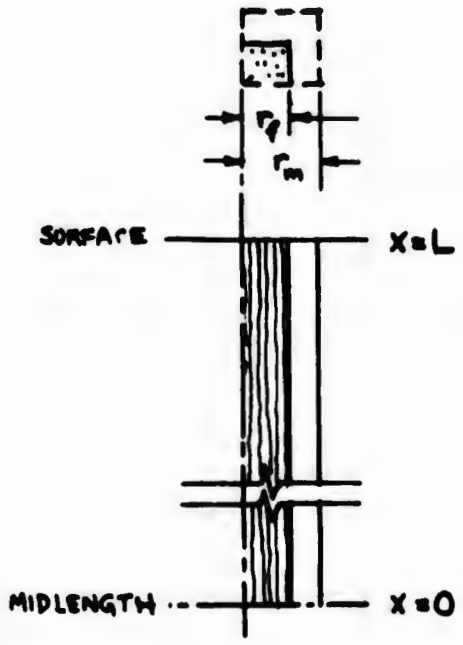

Fig. 2. Unit cell of specimen.

described below defines the stress gradients in terms of a simple shear lag model (adapted from Ref. 3). Once the stresses are defined, the strains and displacements can be calculated for yarn and matrix.

Specifically, we consider simple rectangular bars such as are commonly used for thermal expansion measurements. The symmetry of the situation allows us to do the analysis by studying half the length of such a specimen, considering a single yarn and its surrounding matrix (Fig. 2). Because of the shear lag, the matrix will displace axially more than the yarn, giving rise to a wavy surface at the specimen end. This "roughening" of the surface can produce discrepancies between the measured growth of a specimen and the true thermal expansion of the composite (eg, Ref. 4).

If the interfacial shear stress exceeds the strength of the interface, debonding will occur. In the debonded region, a frictional shear stress can exist, which depends in magnitude on the compressive stress across the interface, among other factors. In the region that remains bonded, the shear stress is predicted from the elastic shear lag analysis. Figures 3 shows schematically the expected relative displacements of yarn and matrix, in the bonded and debonded regions.

We assume the yarns have square cross-sections; it would not be difficult to extend the analysis to rectangular-section yarn bundles, but the major points to be made in this paper can be illustrated with the simpler analysis of square-section reinforcements. Many of the equations for circular-section reinforcements are identical to those for square-section yarns; thus, much of the analysis is also applicable to shear lag between circular fibers and matrix within a yarn bundle.

Shear Lag Equations

For a specimen that is uniformly heated without any external forces, stress equilibrium requires the axial forces in yarn and matrix to sum to zero at every axial location:

$$\sigma_f r_f^2 + \sigma_m (r_m^2 - r_f^2) = 0 \qquad (1)$$

We assume, in accordance with the level of this analysis, that σ_f and σ_m do not vary with radial position.

Consideration of equilibrium, between shear stress and axial stress in the fiber, gives:

$$\tau_f = -\frac{1}{2} r \frac{d\sigma_f}{dx} \quad , \; r \le r_f \qquad (2)$$

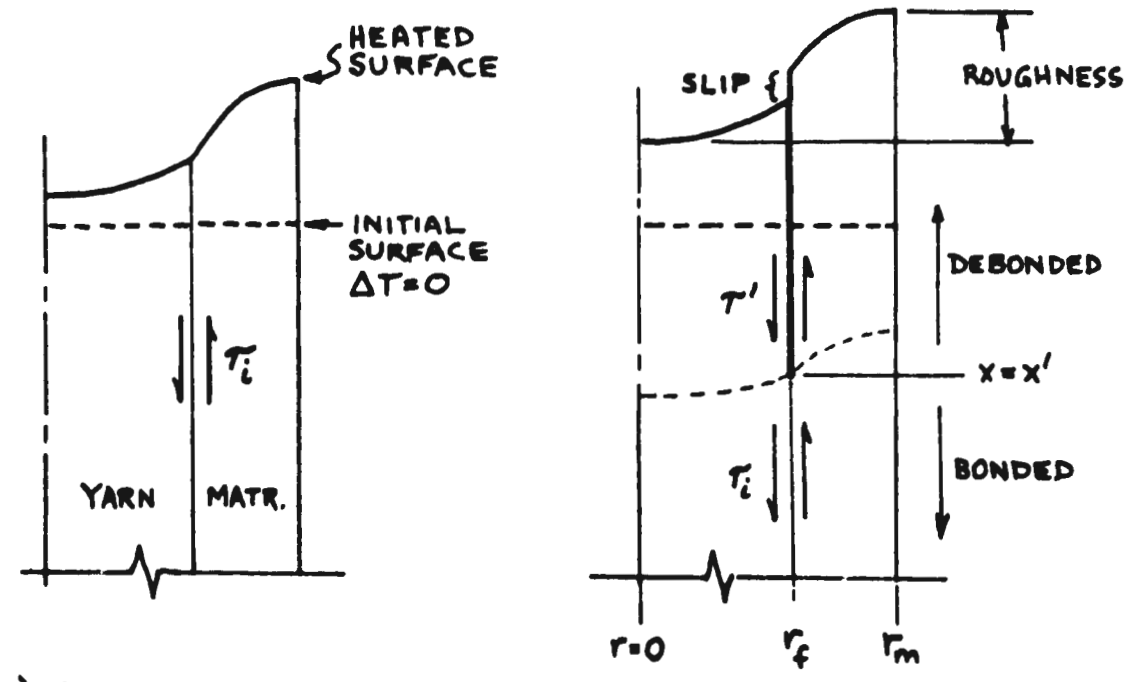

Fig. 3. Schematic of deformations at the free surface.

For the matrix, equilibrium requires:

$$\tau_m = \frac{r_m^2 - r^2}{2r} \frac{d\sigma_m}{dx} \quad , \quad r_f \le r \le r_m \tag{3}$$

or, applying Eq. 1 and introducing the yarn volume fraction, S^2:

$$\tau_m = -\frac{r_m^2 - r^2}{2r} \left(\frac{S^2}{1-S^2}\right) \frac{d\sigma_f}{dx} \tag{4}$$

The shear stress reaches a maximum, for each axial location, at the interface:

$$\tau_i = -\frac{r_f}{2} \frac{d\sigma_f}{dx} \tag{5}$$

When the interface is intact, and the yarn and matrix behave elastically, we may define an average shear strain:

$$\bar{\gamma} = \frac{u_m - u_f}{r_m} \tag{6}$$

which can be related by Hooke's law, to the interface shear stress:

$$\tau_i = G\,\bar{\gamma} \tag{7}$$

Here, G is an "effective" shear modulus that represents the fiber and matrix in appropriate proportions and accounts for our use of maximum shear stress in combination with average shear strain. This effective shear modulus may be derived by expressing the average shear strain at given axial location in terms of the average shear strains in yarn and matrix:

$$\bar{\gamma} = \bar{\gamma}_f S + \bar{\gamma}_m (1-S) \tag{8}$$

Applying Hooke's law:

$$\bar{\gamma}_f = \frac{\bar{\tau}_f}{G_f} \qquad \text{and} \qquad \bar{\gamma}_m = \frac{\bar{\tau}_m}{G_m} \tag{9}$$

where the average shear stresses are:

$$\bar{\tau}_f = \frac{1}{r_f} \int_0^{r_f} \tau_f \, dr \tag{10}$$

and

$$\bar{\tau}_m = \frac{1}{r_m - r_f} \int_{r_f}^{r_m} \tau_m \, dr \tag{11}$$

Introducing Eq 2 and 4, and integrating Eq 10 and 11, gives:

$$\bar{\tau}_f = \frac{\tau_i}{2} = -\frac{r_f}{4} \frac{d\sigma_f}{dx} \tag{12}$$

$$\bar{\tau}_m = -\left(\frac{S^2}{1-S^2}\right) \frac{r_m^2}{2(r_m - r_f)} \left[\ln\left(\frac{1}{S}\right) - \frac{(1-S^2)}{2}\right] \frac{d\sigma_f}{dx} \tag{13}$$

The needed expression for effective shear modulus may now be obtained by substituting Equations 12, 13, 9, and 8 into Eq 7:

$$G = \left[\frac{S}{2G_f} + \left(\frac{S}{1-S^2}\right) \frac{1}{G_m} \left(\ln\left(\frac{1}{S}\right) - \frac{1-S^2}{2}\right)\right]^{-1} \tag{14}$$

Usually, G is about 1.5 to 3 times the low bound (uniform microstress) estimate of the composite shear modulus, and may in some cases be larger than the upper bound (uniform microstrain) estimate.

To obtain a solution for interface shear stress as a function of axial position, x, we proceed by differentiating Eq. 7:

$$\frac{d\tau_i}{dx} = \frac{G}{r_m} (e_m - e_f) \tag{15}$$

where the total strains, e_f and e_m are the sums of mechanical and thermal strains:

$$e_f = \frac{\sigma_f}{E_f} + \alpha_f \Delta T$$

$$e_m = \frac{\sigma_m}{E_m} + \alpha_m \Delta T \tag{16}$$

Substituting Eq 16 and 1 into Eq 15, we get:

$$\frac{d\tau_i}{dx} = \frac{G}{r_m} \left[(\alpha_m - \alpha_f)\Delta T - \frac{\sigma_f}{\beta}\right] \tag{17}$$

where

$$\beta = \frac{E_f}{1 + \frac{S^2}{1-S^2} \frac{E_f}{E_m}} \tag{18}$$

The maximum yarn stress that can be generated by heating alone will occur at the midlength of a very long composite body, where $d\tau_i/dx$ will be essentially zero at midlength. From Eq 17, the maximum yarn stress σ_f^* would be:

$$\sigma_f^* = \beta(\alpha_m - \alpha_f)\Delta T \tag{19}$$

Substituting Eq 19 into Eq 17, and differentiating again, we get:

$$\frac{d^2\tau_i}{dx^2} = -\frac{d\sigma_f}{dx} \left(\frac{G}{\sigma_f^* r_m}\right)(\alpha_m - \alpha_f)\Delta T \tag{20}$$

Substituting the equilibrium condition of Eq 5 gives us a differential equation in τ_i :

$$\frac{d^2\tau_i}{dx^2} - \eta^2 \tau_i = 0 \tag{21}$$

where

$$\eta^2 = \frac{2G}{r_m r_f \beta} \tag{22}$$

A general solution to Eq 21 is:

$$\tau_i = A \sinh(\eta x) + B \cosh(\eta x) \tag{23}$$

where A and B are constants that depend on the boundary conditions. We can readily show B = 0 because the interface shear stress τ_i must be zero at x = 0 (because of symmetry of the specimen). Thus:

$$\tau_i = A \sinh(\eta x) \tag{24}$$

and

$$\frac{d\tau_i}{dx} = \eta A \cosh(\eta x) \tag{25}$$

For a specimen of finite length, the gradient $d\tau_i/dx$ at midlength will not, in general, be zero. Thus, the actual maximum yarn stress (at x = 0) can be expressed as:

$$\sigma_{f_o} = \phi_o \sigma_f^* \quad , \qquad \phi_o < 1 \tag{26}$$

Equating Eq 25 and 17, at x = 0, and using Eq 26, we get a definition of A:

$$A = \frac{1}{\eta}\frac{d\tau_i}{dx}\bigg|_{x=0} = \frac{G_1}{\eta r_m}(\alpha_m - \alpha_f)\Delta T(1-\phi_o) \tag{27}$$

At this point, ϕ_o is undefined. To proceed, we return to consideration of the axial stress in the yarn. From Eq 5 and 26:

$$\sigma_f - \phi_o \sigma_f^* = -\frac{2}{r_f}\int_o^x \tau_i \, dx \tag{28}$$

Introducing Eq 24 and integrating:

$$\sigma_f = \phi_o \sigma_f^* - \frac{2A}{\eta r_f}\left[\cosh(\eta x) - 1\right] \tag{29}$$

The yarn axial stress σ_f' at the end of the elastic region (x = x') may be estimated and used in Eq 29 to provide a second relation between A and ϕ_o:

$$A = \frac{(\phi_o \sigma_f^* - \sigma_f')\eta r_f}{2(\cosh(\eta x') - 1)} \tag{30}$$

If no debonding occurs in the specimen, and it behaves elastically over its entire length, the fiber stress at the end of the elastic region (x = L) is zero. If debonding does occur, the fiber stress at the end of the bonded region (x = x' < L) is given by Eq 41 (derived in the next Subsection).

We solve for ϕ_o by equating Eq 27 and Eq 30:

$$\phi_o = \frac{\sigma_f' - 1}{\sigma_f^*}\operatorname{sech}(\eta x') + 1 \tag{31}$$

In this analysis, we solve for x' numerically by requiring that the shear stress at x' be the interfacial shear strength. An iterative procedure first assumes an arbitrary value of x', solves for ϕ_o and A, computes the elastic shear stress at x' from Eq 24, and if that value does not equal the shear strength (from Eq 49, below), assumes a new value of x' and repeats the calculation and so on until the discrepancy is negligible (less than one percent of the shear strength).

The change in length of the matrix, in the bonded region, is:

$$^{el}u_m = \int_0^{x'} e_m \, dx = x'\alpha_m \Delta T + \int_0^{x'} \frac{\sigma_m}{E_m} dx \tag{32}$$

Introducing Eq 1 and 29, and performing the integration, we get:

$$^{el}u_m = x'\alpha_m \Delta T + \frac{S^2}{E_m(1-S^2)}\left[x'\left(\phi_o \sigma_f^* + \frac{2A}{\eta r_f}\right) - \frac{2A}{\eta^2 r_f}\sinh(\eta x')\right] \tag{33}$$

The corresponding length change of yarn, in the bonded region, may, with the aid of Eq 6, be estimated as:

$$^{el}u_f = {}^{el}u_m - r_m\bar{\gamma} = {}^{el}u_m - \frac{r_m A \sinh(\eta x')}{G_1} \tag{34}$$

Frictional Shear Stress

If the elastic shear stress at the primary yarn interface exceeds the interface shear strength, debonding will occur and the yarn may slip relative to the matrix. A frictional shear stress will exist at the interface. We assume this frictional shear stress τ' is the sum of two factors, the product of a friction coefficient μ and the compressive stress σ_c acting across the interface, and a constant τ^* representing resistance by other effects, such as mechanical interlocking between rough interface surfaces:

$$\tau' = \tau^* - \mu\sigma_c \tag{35}$$

The transverse compressive stress arises from the minimechanical interactions between the transverse yarns and the rest of the composite (which includes our primary axial yarn). Because shear lag phenomena apply also to the transverse yarns, the compression will vary with distance from a

transverse free surface. At a transverse surface, the compressive stress on the primary yarn will approach zero. Toward the center of a large enough body, the compressive stress will approach a maximum value σ_c^* that, for each set of transverse yarns may be estimated as (eg, Ref 2):

$$ {}^{j}\sigma_c^* = E_{fT}\left(\bar{\alpha}_j - \alpha_{fT}\right)\Delta T \tag{36} $$

where $\bar{\alpha}_j$ is the composite's thermal expansion:

$$ \bar{\alpha}_j = \frac{\alpha_f E_f v_j + \alpha_m E_m (1 - v_j)}{E_f v_j + E_m (1 - v_j)} \tag{37} $$

and v_j is the yarn volume fraction in the appropriate direction. For illustrative purposes, we simplify the analysis to deal only with square primary yarns in a matrix characterized by equal distribution of yarns in the two transverse directions. Then:

$$ \sigma_c^* = E_{fT}\,\Delta T\left(\frac{\alpha_f E_f v_T + \alpha_m E_m (1 - v_T)}{E_f v_T + E_m (1 - v_T)}\right) \tag{38} $$

where

$$ v_T = \frac{v_y - s^2}{2} \tag{39} $$

and v_T is the total volume fraction of yarn in the composite, usually in the vicinity of .7 to .75. The task of estimating the compressive stress distribution in a slender bar specimen is not trivial as it would require iterative application of the shear lag analysis to the primary and transverse yarns. To illustrate the effects, we define a factor ψ :

$$ \sigma_c = \psi \sigma_c^* \quad , \qquad \psi \leq 1 \tag{40} $$

and we consider two examples in the application of the analysis: 1) ψ = 0.1 as applying approximately to the corners of a specimen, and 2) ψ = 1.0 (maximum compression) as providing a bound to the situation at the specimen centerline (Figure 4).

We assume further that the frictional shear stress is invariant with axial position. Then, by integrating Eq. 5, we find the distribution of axial stress in the yarn to be:

$$ \sigma_f = \frac{2\tau'}{r_f}\left(L - x\right) \quad , \quad x \geq x' \tag{41} $$

The change in length of the yarn in the debonded region is:

$$ {}^{fr}u_f = \int_{x'}^{L} e_f\, dx \tag{42} $$

and the length change of matrix is:

$$ {}^{fr}u_m = \int_{x'}^{L} e_m\, dx \tag{43} $$

Performing the integrations, we get:

$$ {}^{fr}u_f = \alpha_f \Delta T\left(L - x'\right) + \frac{\tau'}{r_f E_f}\left(L - x'\right)^2 \tag{44} $$

and

$$ {}^{fr}u_m = \alpha_m \Delta T\left(L - x'\right) - \frac{\tau'}{r_f E_m}\left(\frac{s^2}{1 - s^2}\right)\left(L - x'\right)^2 \tag{45} $$

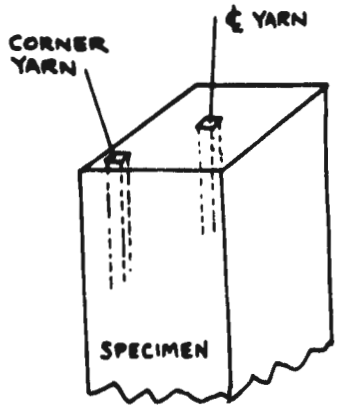

Fig. 4. Yarn positions.

Total Length Change of the Specimen on Heating

From Eq 44 and 45, and Eq 33 and 34, it is clear that the length change measured in a thermal expansion test will depend on whether the test technique reads the length change of the matrix or of the yarn. The total length change of the matrix region is the sum of the length changes in the bonded and debonded regions:

$$ u_m^* = {}^{el}u_m + {}^{fr}u_m \tag{46} $$

Similarly, the total length change of the yarn is:

$$ u_f^* = {}^{el}u_f + {}^{fr}u_f \tag{47} $$

The difference between these two length changes is the surface roughening shown in Figure 3.

INPUT PROPERTIES

The illustrative results presented later are intended to represent graphitized 3D carbon-carbon material made with T-300 yarns with pitch densification, such as used in the 7-inch and 15-inch billet programs (Ref. 5 and 6). This section describes the approach to estimating the material properties used in the analysis. The values used to produce the illustrative results (next Section) are listed in Table 1.

The axial modulus and thermal expansion of the yarn phase are derived from test data. For modulus, the correlation by F. I. Clayton, reported in Ref. 6, provides estimates of in-situ filament modulus Efil vs. temperature. We assume the yarn is composed of 60 percent filament by volume, so that Ef ≅ .6 x Efil. For axial thermal expansion of the yarn, we use directly the data obtained by Lander (Ref. 7) on a specimen comprising a single yarn bundle.

The transverse expansion of the matrix phase (that includes the transverse yarns and matrix pockets) is based directly on the measurements by Lander (Ref. 7) on a specimen from which the axial yarns were excised.

The remaining properties of the matrix phase and of the yarn are estimated using simple rule-of-mixtures equations from values for filaments and pitch-precursor matrix recommended by Kibler (eg, Ref. 8). Estimates are required here because direct experimental data are unavailable.

Graphitized 3D carbon-carbons are known to have a regularly cracked microstructure (Ref. 2, for example). In the current context, the existence of these microcracks affects the thermo-elastic properties of the matrix region, the transverse elastic properties of the yarn, and the effective shear modulus used in the shear lag analysis. The simplest approach to accounting for the microcracks is to assign efficiency factors to the extensional and shear moduli of the matrix material (eg, Ref. 8 and 9):

$$\eta_E = \frac{E_m}{E_m^*} = \frac{E_{fT}}{E_{fT}^*} \qquad \eta_S = \frac{G_m}{G_m^*} = \frac{G_f}{G_f^*} \tag{48}$$

where the "starred" properties represent uncracked material. Following the recommendation of Ref. 9, we assign a lower efficiency to the extensional behavior than to the shear behavior. From Kibler's work, we use a shear efficiency factor of 0.4. From attempts to match some of Lander's thermal expansion data (Ref. 7), it appears that the extensional efficiency factor is in the vicinity of .05 to .10.

Data for interfacial shear strength and friction coefficients is lacking. From a brief review of related information (eg, pull-out failures in tensile tests, microshear data, shear tests of 1D and 2D composites, and friction coefficients measured at room temperature between composite parts) approximate values were estimated. The values used in the illustrative calculations are listed in Table 1.

The input value for shear strength, τ_{EL}^*, represents the strength in the absence of substantial compression across the interface. For high values of σ_c it is possible that the estimated friction shear stress (Eq 35) will be greater than the input shear strength. While other approaches are also attractive (eg, use of a multiaxial fracture criterion for shear strength), in this paper we take the effective elastic shear strength, τ_{EL}, to be the larger of the input strength and the estimated friction shear stress:

$$\tau_{EL} = \text{MAX}\left[\tau_{EL}^*, \tau'\right] \tag{49}$$

TABLE 1. INPUTS TO ILLUSTRATIVE ANALYSIS

PROPERTY			VALUE AT TEMPERATURE				
		Temp, F	0	1000	2000	3000	4000
shear modulus, yarn	psi	Gf*	1.50E+06	1.51E+06	1.60E+06	1.71E+06	1.49E+06
shear mod, transverse composite	psi	Gm*	5.36E+05	5.43E+05	5.75E+05	6.12E+05	5.34E+05
Young's modulus, yarn, axial	psi	Ef	3.60E+07	3.60E+07	3.60E+07	2.40E+07	2.10E+07
Young's modulus, yarn, transverse	psi	EfT*	1.38E+06	1.41E+06	1.50E+06	1.61E+06	1.42E+06
Young's modulus, transv. composite	psi	Em*	1.38E+06	1.41E+06	1.50E+06	1.61E+06	1.42E+06
extensional bond efficiency		etaE	0.05	0.05	0.05	0.05	0.05
shear bond efficiency		etaS	0.40	0.40	0.40	0.40	0.40
CTE, yarn, axial	per F	alpf	0.00E+00	-2.00E-07	2.00E-07	4.00E-07	5.50E-07
CTE, yarn, transverse	per F	alpfT	0.00E+00	4.64E-06	4.46E-06	4.33E-06	4.89E-06
CTE, transverse composite	per F	alpm	0.00E+00	1.60E-06	2.25E-06	3.00E-06	3.75E-06
nominal interface shear strength	psi	tauEL*	1000	1000	1000	1000	1000
minimum frictional shear strength	psi	tau'	200	200	200	200	200
coeff. friction		mu	0.3	0.3	0.3	0.3	0.3
total yarn volume fraction		vY	0.75	0.750	0.750	0.750	0.750

ILLUSTRATIVE RESULTS

The shear lag analysis is applied here to the prediction of thermal expansion data as a function of the technique used for measurement of specimen length change. The various specimen configurations and length measurements used for 3D carbon-carbons are sketched in Figure 5.

The first example deals with analysis of "matrix" expansion u_m^* and yarn expansion u_f^*, providing calculations that may be compared to Lander's data (Ref. 7) for flat-ended and protruding-yarn specimens, respectively. Lander tested 2-inch long specimens taken from the outer-diameter region of a woven cylindrical billet, oriented in the billet's axial direction. We used the input properties shown in Table 1 and implemented the analysis using an estimated yarn volume fraction of 0.19 and a unit-cell radial dimension, r_m, of .07 inch. Figure 6 shows the analytical predictions to be in reasonable agreement with Lander's data up to about 2200 C (4000 F). Correlations above 4000 F were not attempted because the analysis does not currently include creep/relaxation effects, which are important at higher temperatures.

The predictions are shown as lines in Figure 6; the top solid line is the prediction for the corner of a flat specimen where the frictional stress is reduced because minimal compression can exist across the yarn interface; the bottom solid line is the prediction for the centerline region of a flat specimen that is sufficiently large in cross-section to exhibit maximum compression at the yarn interface. The lines tend to bracket Lander's data, suggesting that the analytical model is capable of predicting the major effects in such specimens. Also shown is the predicted response of the yarn, which corresponds to data from protruding-yarn specimens. The difference between predicted responses of yarns at the corner and centerline is negligible, so only one dotted line is plotted. In Figure 7, these predictions are compared to the theoretical response of the bulk composite (estimated by Eq 37); we see that the yarn responses are quite close to the theoretical value, whereas the matrix response is a substantial overestimate.

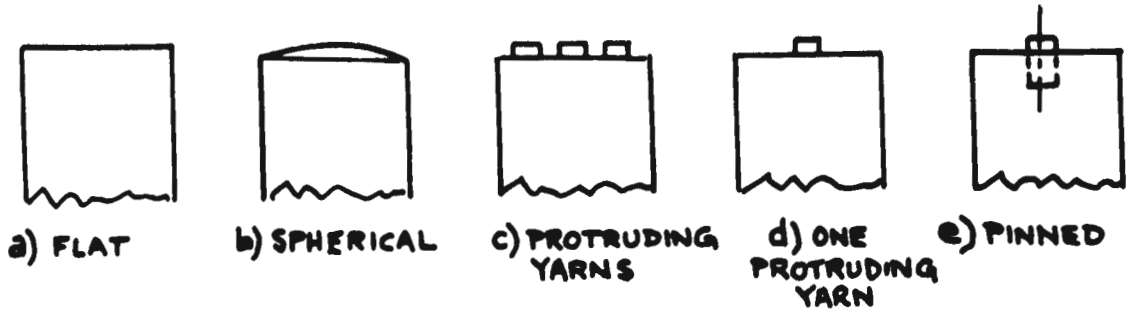

Fig. 5. Various end configurations used in thermal expansion testing.

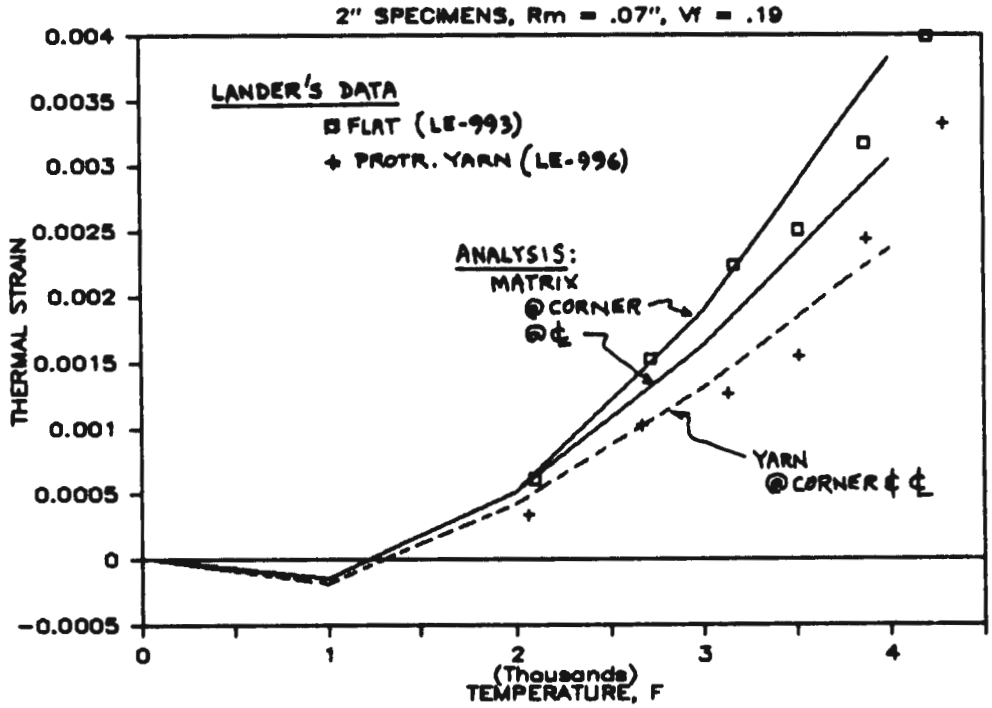

Fig. 6. Comparison of analysis to Lander's data for flat and protruding-yarn specimens.

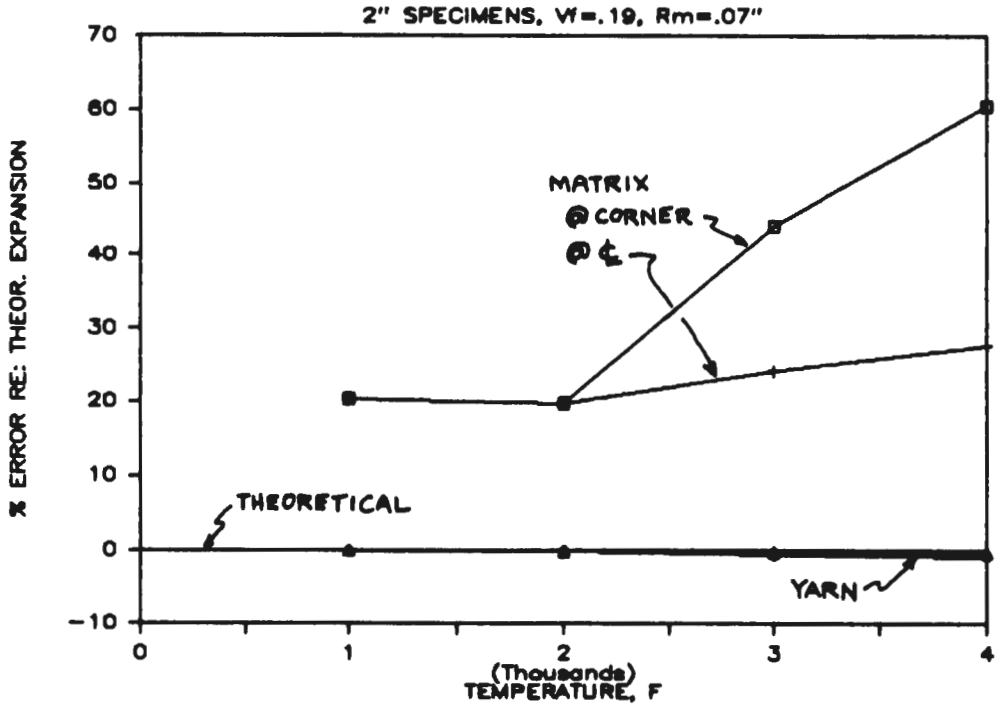

Fig. 7. Discrepancies between predicted measurements and theoretical expansion of bulk composite.

Figure 8 shows the predicted roughening (in hundredths of an inch) of a flat end-surface and the predicted extent of debonding. Figure 9 shows the predicted variation of yarn axial stress and interface shear stress, for the centerline region.

Additional analyses were done to explore the effects of specimen length (actually, the key variable is the ratio of specimen length to unit-cell dimension, r_m) and yarn volume fraction. For these calculations, we assumed the yarn experiences the maximum transverse compression. Thus the data provide a low-bound expansion for the centerline of flat-ended or spherical-ended specimens. Also, the interface shear strength was taken as 2000 psi, rather than the 1000 psi used in analyzing Lander's data.

The effect of specimen length on predicted expansion data to 4000 F is shown in Figure 10, for a yarn fraction of .21 and a unit-cell radius of .07-inch. We see that the potential errors from using flat-ended specimens decrease as specimen length increases. It may be of interest to note that the specimen lengths used for expansion measurements on fine-weave carbon-carbons (eg, Ref. 10) were sufficient to make such errors nearly negligible; to achieve similar accuracy with the coarse weave composites such as the billet Lander studied, we would need specimen lengths in the order of ten inches. The predicted surface roughening and the length of debond are insensitive to specimen length, in the range studied. The yarn stress generated at the specimen midlength is within one percent of the theoretical value, even for the shortest length shown; this is consistent with the length of the shear-lag region shown in Fig 9. Thus, the assumption of full compression across the centerline yarn interface may be close to reality for specimens about 3/8-inch in cross-section. However, as noted earlier, the proper analysis of the transverse compression is complex, so the implication just stated should viewed cautiously.

The effects of yarn volume fraction on predicted expansion data to 4000 F are shown in Figure 11, for 2-inch long specimens having a unit-cell radius of .07 inch. Potential errors in the use of flat-ended specimens increase significantly at low values of yarn volume fraction. This finding may aid in explaining some of the very high values of radial-direction expansion reported for some cylindrical billet materials (eg, Ref. 6).

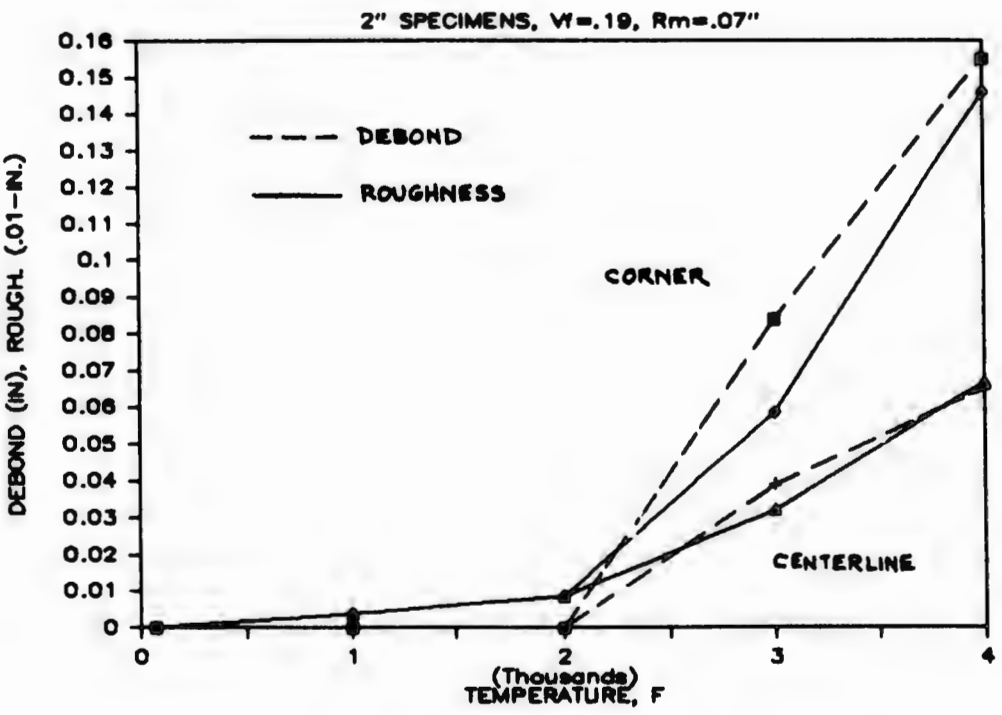

Fig. 8. Predicted extent of debonding and surface roughening at 4000 F in specimens of Fig. 6.

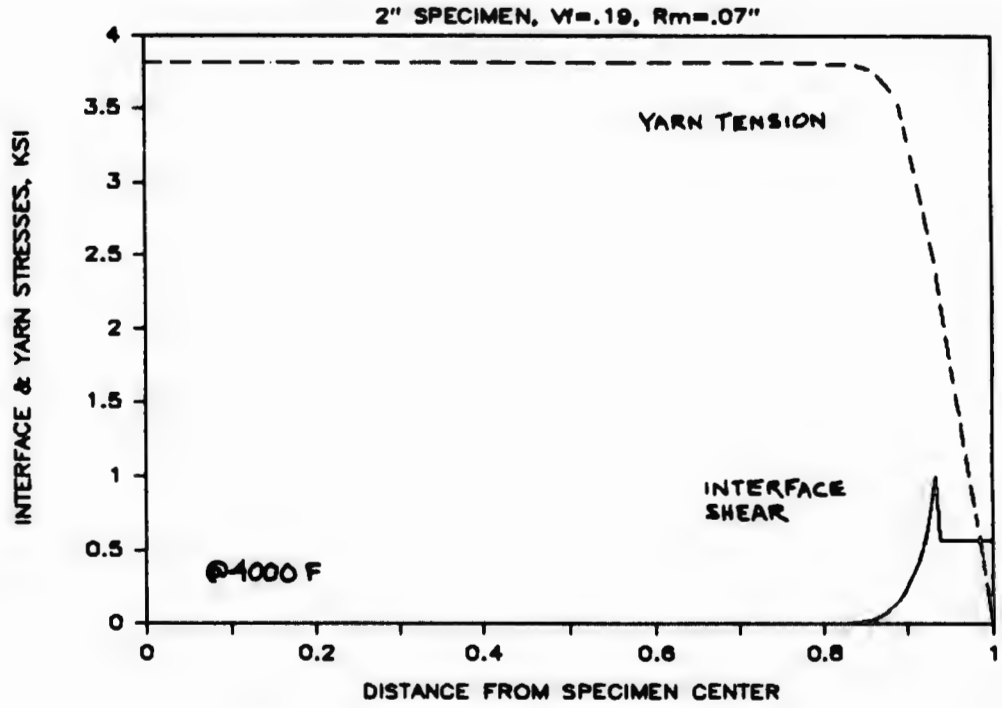

Fig. 9. Predicted stress gradients at interface and in yarn at 4000 F at specimen centerline.

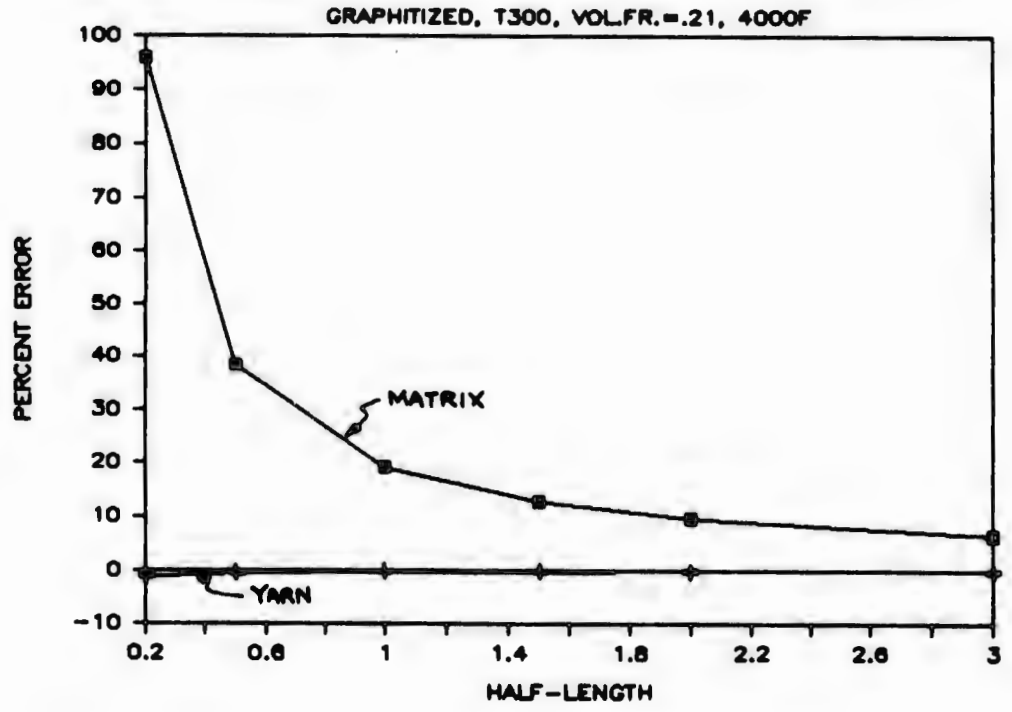

Fig. 10. Effect of specimen half-length on predicted errors at 4000 F.

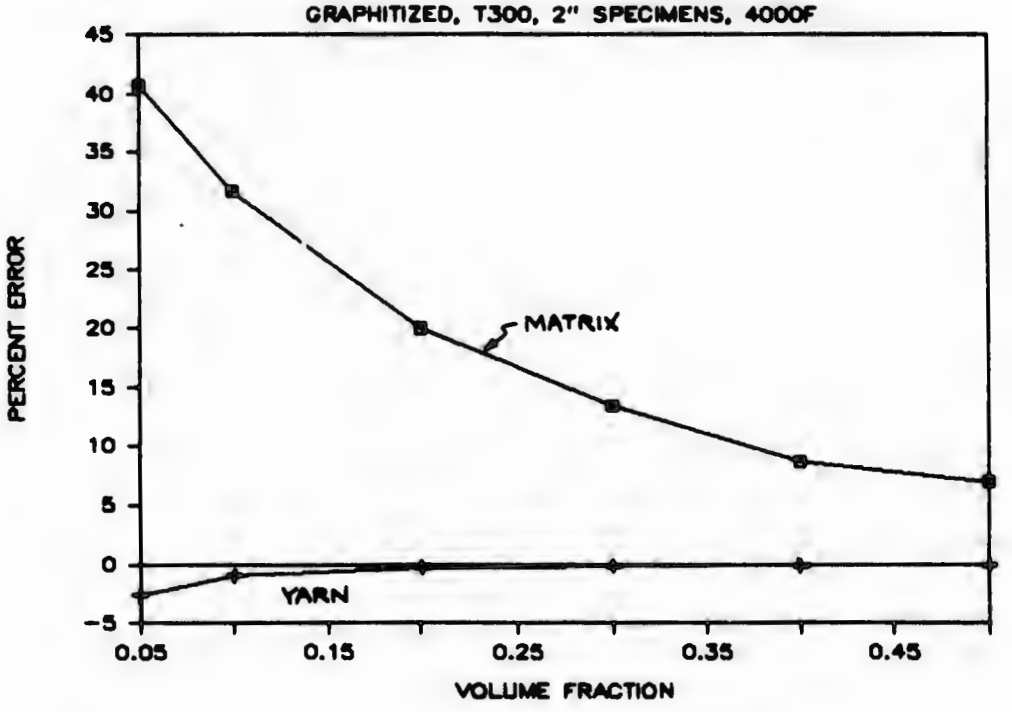

Fig. 11. Effect of yarn volume fraction on predicted errors at 4000 F.

CONCLUDING REMARKS

The shear lag analysis shows that thermal expansion data can be sensitive to the details of the measurement technique, especially to the length of specimen used and to the manner of measuring its change in length (Figure 5). Potential errors are larger for specimens of smaller volume fraction of yarns in the direction of measurement, and for coarse-weave composites.

On the basis of the findings, the use of flat-ended specimens should be discouraged. The use of spherical-end specimens is preferable to flat-end specimens; however, significant error may be experienced due to surface roughening. The use of pin-ended specimens should provide quite accurate data if the pin rests on the end of a yarn and is of a diameter smaller than the yarn cross-section; otherwise, data from pinned specimens may be influenced by roughening at the base of the pin. (The shear lag analysis could readily be extended to treat the effect of pin depth). Of all the configurations shown in Figure 5, the most accurate appears to be the protruding-yarn specimen (Fig. 5c) which was first used by Lander in the end-effects study of Ref. 7.

Many of the properties that are inputs to the analysis are not well known. It is recommended that research be directed toward measuring transverse properties of yarn bundles, in-situ properties of matrix-pocket regions, establishing the appropriate efficiency factors to account for pre-existing microcracks, measuring yarn interface strengths and friction coefficients, all as functions of temperature. While some data of the types listed is available, more is needed for specific materials of interest.

It would be worthwhile to attempt experimental verification of the predicted debond lengths and surface roughenings.

Currently, the analysis does not treat creep/relaxation effects, which are undoubtably important at temperatures above 4000 F. Extension of the analysis, and the acquisition of relevant constituent creep data would be worthwhile. Other extensions of the analysis should also be attempted. These include treatment of rectangular-section yarns, allowance for differing volume fractions for the two sets of transverse yarns, and better treatment of the compressive stresses that influence the frictional shear.

Motivation for the suggested further work includes the belief that shear lag analysis is a powerful tool for studying the structural response of 3D carbon-carbon components near free surfaces. In comparison to finite-element analyses of mini-mechanical interactions, the shear lag approach is simple and inexpensive; the simplifications (including neglect of Poisson's interactions) and lack of rigor (in the sense of elasticity solutions) are compensated for by the ability to treat approximately such phenomena as inter-constituent slip, which are difficult to model rigorously.

NOMENCLATURE

α = thermal expansion coefficient, secant value

γ = shear strain

σ = extensional stress

τ = shear stress

E = Young's modulus

G = shear modulus

L = half the length of the specimen

S = ratio of yarn radius to matrix radius

T = temperature

e = extensional strain, total

r = radial distance, or radius

u = axial displacement

v = volume fraction of yarn

x = axial distance

Subscripts

c = compression

f = pertaining to yarn

i = pertaining to interface

j = index defining a yarn direction

m = pertaining to matrix

T = transverse to the yarn axis

ACKNOWLEDGMENTS

Support of this research by the Office of Naval Research and the encouragement offered by Dr. L. H. Peebles, Jr., ONR's Scientific Officer, are gratefully acknowledged. The author also thanks Mr. Louis L. Lander, of FMI, for valuable discussions of thermal expansion measurement techniques and data interpretation, and for early access to his experimental data.

REFERENCES

1. Greszczuk, L. B., "Analysis of Dimensional Changes and Fiber-Matrix Interactions During Processing of 3D Carbon-Carbon Composites", Extended Abstracts 13th Biennial Conference on Carbon, American Carbon Society, 1977, pp70-71.

2. Jortner, J., Thermal Expansion and Bimodularity of 3D Carbon-Carbon Composites, Annual Report to ONR, Contract N00014-80-C-0717, November 1981.

3. Rosen, B. W., Mechanics of Composite Strengthening, presented at ASM Seminar on Fiber Composite Materials, October 1964.

4. Jortner, J, and Clayton, F. I., "Effects of Free-Surface Roughening on Thermal Expansion Data", JANNAF Rocket Nozzle Materials Report, Vol.1, No.5, August 1979.

5. Ellis, R. A., and Kearney, W. J., Cylindrical Carbon-Carbon ITE (7-in. Billet Program), AFRPL-TR-83-057, November 1983.

6. Ellis, R. A., 3D Carbon-Carbon Billets (15-in. Billet Program), AFRPL-TR-82-042, July 1982.

7. Lander, L. L., Final Report on Mechanical and Thermal Properties of Seven-Inch Man-Tech Billet Program, FMI Report EMTL-MT-83-1592, March 1983. (see Appendix C).

8. Kibler, J. J., et al, Exploratory Development of In-Process Yarn Bundle Properties, AFWAL-TR-80-4096, July 1980. See also Kibler and Chatterjee, Development of a Mini-Mechanics Model for 3-D Carbon-Carbon Composites, MSC Report TFR 7510, 1975.

9. Jortner, J., Thermal and Mechanical Behavior of Carbon-Carbon Composites, Annual Report to ONR, Contract N00014-82-C-0405, January 1984.

10. Littleton, H. E., and Pears, C. D., Mechanical, Thermal and Nondestructive Characterization of GE-2.2.3, AFML-TR-77-48, April 1977.